Biomass and Bioenergy 191 (2024) 107480

Contents lists available at ScienceDirect

Biomass and Bioenergy

journal homepage: www.elsevier.com/locate/biombioe

Hydroprocessing of waste cooking oil to produce liquid fuels over Ni-Mo and Co-Mo supported on carbon nanotubes

K.K. Ferreira [a,b], C. Di Stasi [c], A. Ayala-Cortés [c], L.S. Ribeiro [a,b], J.L. Pinilla [c], I. Suelves [c,**], M.F.R. Pereira [a,b,*]

[a] LSRE-LCM – Laboratory of Separation and Reaction Engineering - Laboratory of Catalysis and Materials, Faculty of Engineering, University of Porto, Rua Dr. Roberto Frias, 4200-465, Porto, Portugal

[b] ALiCE – Associate Laboratory in Chemical Engineering, Faculty of Engineering, University of Porto, Rua Dr. Roberto Frias, 4200-465, Porto, Portugal

[c] Instituto de Carboquímica, CSIC, C/ Miguel Luesma Castán 4, Zaragoza, 50018, Spain

ARTICLE INFO

Keywords:
Hydrodeoxygenation
Ni-Mo and Co-Mo catalysts
Carbon nanotubes
Jet and diesel fuel
Waste cooking oil valorization

ABSTRACT

New fuel production alternatives are becoming increasingly necessary to replace fossil energy sources and reduce the environmental implications of carbon emissions. In this context, renewable sources, such as waste cooking oil (WCO), are an excellent choice for producing bio-based fuels. However, to use WCO as fuel, the oxygen content in its triglyceride structures must be removed. To this end, bimetallic Co-Mo and Ni-Mo supported on pristine carbon nanotubes (CNT) and oxidized carbon nanotubes (CNT_{ox}) were synthesized to investigate the hydroprocessing of WCO in a batch reactor operating at 350 °C, 70 bar of H_2 (evaluated at ambient temperature) for 3 h. The results showed that Ni-Mo/CNT_{ox} exhibited superior catalytic performance, mainly producing *n*-alkanes in the range of C_{14}-C_{22} with a carbon conversion of about 67 mol.% and being selective for light alkanes (6.6 mol.% of C_5-C_7), jet fuel (11.4 mol.% of C_8-C_{16}) and diesel fuel (81.2 mol.% of C_{17}-C_{22}). On the other hand, a residence time of 5 h was necessary to achieve the same results with the carbon-supported Co-Mo catalysts. Hydrodeoxygenation was the main deoxygenation route followed using CNT based catalysts.

1. Introduction

In response to global environmental and energy issues, the quest for sustainable and renewable energy sources has become more intense in recent years. In 2022, CO_2 emissions from the transport sector were approximately 8 Gt and the desired outlook for 2030 is a 25 % reduction in emissions [1]. Considering the essential factors for reducing environmental impacts in accordance with climate agreements, the development of alternative technologies to produce renewable fuels is increasingly emerging. In this context, the reuse of waste to create new products becomes more prominent in relation to the circular economy principles.

Waste cooking oil (WCO) is a lipid-promising renewable source because it contains triglycerides and free fatty acids with a hydrocarbon range between C_{16} – C_{22} [2]. Its use as a precursor of biodiesel by transesterification has been widely explored through the past decades [3–6]. However, WCO could be also converted into other liquid fuel ranges by hydrotreatment processes [7–11]. To obtain gasoline (C_4-C_{12}), aviation fuel (C_8-C_{16}), or diesel fuel (C_{15}-C_{24}), the WCO must undergo deoxygenation, cracking, and isomerization reactions [12]. In this regard, the deoxygenation stage is critical for eliminating the oxygen contained in the triglycerides and free fatty acids of WCO, which decrease its performance as a fuel by lowering its oxidative stability, increasing its overall acidity and viscosity, and lowering its heating value [12,13]. The removal of oxygen atoms can pursue different routes such as hydrodeoxygenation (HDO), decarboxylation (DCO_2) and decarbonylation (DCO), producing as by-products water (H_2O), carbon dioxide (CO_2) and carbon monoxide (CO), respectively [12,14].

Both the presence of hydrogen and catalysts are critical to these reactions. Bimetallic catalysts based on transition metals (e.g., Ni, Co, Mo, W) supported on γ-Al_2O_3 are used on a large scale in the petrochemical industry to remove heteroatoms (S, N and O). To achieve the appropriate molecular cracking and isomerization, the support must also have the proper physical and chemical characteristics. Acid catalytic supports are

* Corresponding author. LSRE-LCM – Laboratory of Separation and Reaction Engineering - Laboratory of Catalysis and Materials, Faculty of Engineering, University of Porto, Rua Dr. Roberto Frias, 4200-465, Porto, Portugal.

** Corresponding author.

E-mail addresses: isuelves@icb.csic.es (I. Suelves), fpereira@fe.up.pt (M.F.R. Pereira).

https://doi.org/10.1016/j.biombioe.2024.107480

Received 18 September 2024; Received in revised form 29 October 2024; Accepted 4 November 2024

0961-9534/© 2024 The Authors. Published by Elsevier Ltd. This is an open access article under the CC BY-NC license (http://creativecommons.org/licenses/by-nc/4.0/).

frequently employed [15–17]. Furthermore, mesopores are desirable for preventing restrictions on internal mass transfer. Currently, carbon nanotubes (CNTs) have been gaining attention in catalytic applications for their outstanding properties due to their tubular graphitic nanostructure [18–20]. They are based on a hexagonal lattice of sp^2 carbon atoms such as graphene. Their electrical and mechanical stability, high surface area and pore volume make CNTs an outstanding material for catalytic applications [21]. Those last textural properties facilitate the metal dispersion as well as the diffusion of reagents and products into the active sites, due to the absence of micropores. Additionally, CNTs have high thermal stability and tunable chemical nature. For instance, CNTs oxidation with acid is an effective way to introduce oxygenated groups on their surface, adjusting the acidity and enhancing metal phase dispersion. With all of the advantages of CNTs, this carbon material is an excellent candidate to be used as catalyst support for the hydroprocessing of WCO [18,21].

Besides the superior features of CNTs, research of non-edible feedstock as WCO using this class of materials is scarce in the literature. In the past decade, many studies concentrated their efforts on investigating catalysts. For example, spent fluid catalytic cracking (SFCC) [8], heterogeneous catalysts derived from bull bones [9], sulfide Ni-Mo/silica-alumina [22], commercial SO_4^{2-}-Fe_2O_3/Al_2O_3 [23], CaO – L_2O_3/activated carbon [24] and Ni supported on different zeolites [7] were employed in the conversion of WCO into biodiesel and other fuel range hydrocarbons. Few research applied original or modified CNTs as supports, such as Ahranjani et al. [25] which used CNTs coated with magnetic iron oxide and doped with cadmium oxide (CdO) to convert WCO in biodiesel by transesterification. Other works assessed bimetallic Ni/Co-Mo using CNTs as support for the conversion of vegetable oils and model compounds from lipid sources (such as fatty acids and phenols) [20,26,27].

The present work aimed to evaluate the conversion of WCO into liquid fuels using bimetallic Co-Mo and Ni-Mo catalysts supported on CNTs (CNT) and oxidized CNTs (CNT_{ox}). To the best of our knowledge, WCO hydroprocessing using CNT-supported catalysts is poorly reported in the literature. A catalytic screening of the developed catalysts was carried out. In addition, based on the analysis of the products, the reaction pathway of the WCO deoxygenation was proposed.

2. Material and methods

2.1. Chemicals and materials

Multi-walled CNT (Nanocyl-7000, purity of 90 %) and *n*-decane (99 %) were purchased from Nanocyl and Sigma Aldrich, respectively. The metal precursors $(NH_4)_6Mo_7O_{24}$ (99.7 %), $Co(NO_3)_2{\bullet}6H_2O$ (99 %) and $Ni(NO_3)_2$ $\bullet 6H_2O$ (99 %) were purchased from VWR. Commercial Co-Mo/Al_2O_3 was acquired from Alfa Aesar. WCO was provided by *Naturalmente Social Recikla, S. L.* (Zaragoza, Spain).

2.2. Catalysts preparation

CNT and CNT_{ox} were used as support materials. The oxidation procedure was carried out to introduce oxygenate groups on the CNTs surface thus improving metals dispersion. This treatment also enhances the catalyst acidity, which is beneficial for the promotion of isomerization/cracking reactions. Briefly, the material was put in contact with HNO_3 (7 mol L^{-1}) and heated to the boiling temperature for 3 h. Following that, the obtained material was rinsed with distilled water until neutral pH and dried at 110 °C for 24 h (CNT_{ox}). Bimetallic catalysts with nominal metal loadings of 2.5 wt% of Co or Ni and 10.5 wt% of Mo were prepared by incipient wetness impregnation using an aqueous solution of the corresponding metallic precursors, added dropwise to each support material. After the impregnation, the materials were dried overnight at 110 °C in an oven and then subjected to a thermal treatment in a tubular furnace under N_2 flow for 3 h followed by reduction under pure H_2 flow for 3 h at 600 °C and 550 °C for Co-Mo and Ni-Mo catalysts, respectively. The commercial catalyst Co-Mo/Al_2O_3 was calcined and reduced in a tubular furnace under H_2 flow for 3 h at 600 °C. The prepared catalysts were denoted as Co-Mo/CNT, Co-Mo/CNT_{ox} Ni-Mo/CNT and Ni-Mo/CNT_{ox}.

2.3. WCO characterization

The carbon content of the WCO used was determined by elemental analysis using a Thermo Electron Flash 1112 Analyser.

To analyze the fatty acid content, a transesterification procedure was adopted [28]. In brief, the transesterification involved 1.5 g of KOH, 120 mL of CH_3OH, and 200 mL of WCO. Initially, KOH was dissolved in CH_3OH at 50 °C and, after its complete dissolution, pre-heated WCO was added, and the solution was stirred for 60 min at 800 rpm. The resulting product was then separated from the glycerol phase and subsequently analysed by gas chromatography.

2.4. Catalyst characterization

The textural properties of the supports and catalysts were established by N_2 adsorption isotherms at – 196 °C. First, the samples were degassed at 150 °C for 3 h under vacuum and the analyses were performed in a Quantachrome NOVA 4200e Surface Area and Pore Size analyser. Total specific surface areas were determined according to the Brunauer–Emmett–Teller method (S_{BET}), the external surface areas (S_{ext}) were determined by the *t*-method, while the total pore volumes (V_p) were calculated from the amount of N_2 adsorbed at $P/P_0 = 0.98$.

The powder X-ray diffraction (XRD) patterns of the catalysts were collected on a Philips X'Pert MPD diffractometer (Cu-Kα = 0.15406 nm). The diffracted intensity of Cu-Kα radiation was measured in the 2θ range between 10° and 100°.

Transmission electron microscopy (TEM) and scanning transmission electron microscopy (STEM) images were taken using a Tecnai F30, FEI company, at 300 kV filament voltage, which allows a maximum point resolution of (1.5 Å). The catalyst samples were prepared by depositing them onto carbon-coated 400-mesh copper grids after suspending them in water under ultrasound.

Co, Ni and Mo contents were obtained by inductively coupled plasma-optical emission spectroscopy (ICP-OES) using the ICPE-9000 spectrometer (Shimadzu). Elemental analysis was performed to determine the amount of carbon, hydrogen, nitrogen, and sulphur using a Vario Micro Analysis CHNS (at 1050 °C) and oxygen was measured using OXY cube analyser (at 1450 °C). The standard deviation values for C, H, O, Co, Ni and Mo are presented in Table S1.

Chemical titration was used for the calculation of the number of acidic groups on the catalysts' surface, using the following procedure: 100 mg of catalyst and 20 mL of 0.05 M NaOH solution were stirred for 1 h. Afterward, each filtrate was pipetted, and the excess base was titrated with 0.05 M HCl.

2.5. Catalytic deoxygenation of WCO

Before HDO experiments, an initial treatment (degumming) was performed to eliminate phospholipids from the liquid. Firstly, 450 mL of WCO were heated up to 80 °C and, once the desired temperature was reached, 4 vol% of water was added. The mixture was then let to settle for 24 h through decantation. Finally, the undesired fraction containing the phospholipids was removed, and the resulting purified oil was collected.

The catalytic tests were carried out in a 100 mL stainless steel autoclave batch reactor (Ilshin Autoclave). In a typical run, 2.5 g of WCO were diluted in 25 g of *n*-decane, which was subsequently fitted with 0.25 g of catalyst. After purging three times the reactor with N_2, the initial H_2 pressure of 70 bar (at room temperature) was adjusted. The reactions were performed at 350 °C, with a stirring rate of 1000 rpm and

3 h of residence time, considered as the time after the target temperature was reached. At the end of each run, the reactor was immediately quenched in cold water until room temperature; subsequently, gas and liquid samples were collected to analyze the reaction products. In addition, experiments without catalyst and the supports (CNT and CNT_{ox}) without active phases were performed to assess the background activity and the catalytic effect on the deoxygenation of WCO, respectively.

The liquid phase was analysed by a CLARUS 580 (PerkinElmer) gas chromatograph equipped with a flame ionization detector (GC-FID) and an Elite-5 column of 30 m length and 250 μm diameter (Crossbond: 5 % diphenyl - 95 % dimethylpolysiloxane). To confirm the components identified, the chemical composition was also analysed by a PerkinElmer Chromatograph (GC, Clarus® 690) (Waltham, MA, USA) gas chromatography coupled to mass-spectrometry (GC-MS). The gas products were analysed by a Refinery Gas Analyser Model 1157 (PerkinElmer) coupled with FID and a dual thermal conductivity detector (TCD).

Since the triglycerides present in WCO cannot be quantified and identified by GC-FID and GC-MS, the conversion (X_C) was estimated using Eq. (1), where $n_{C_{WCO}}$ is the carbon moles content in the WCO fed to the reactor (from the CHNS analysis of WCO) and n_{C_i} is the number of carbon moles in each identified compound in the final liquid and gas products. The product distribution was evaluated through the definition of selectivity of a compound *i* as in Eq. (2). The experiments were carried out in duplicate, and the standard deviations associated with the conversion were ±1.5 %, while those of the selectivity of each compound were below 5 % and are better elucidated in Table S2. Associated errors with n-C_5-C_7, n-C_8-C_{16}, n-C_{17}-C_{22}, iso-alkanes and alkenes selectivity are 3.5, 4.2, 3.1, 0.7 and 1.3 % respectively.

$$X_C = \frac{\sum n_{C_i}}{n_{C_{WCO}}} \times 100 \quad (1)$$

$$S_i = \frac{\text{moles of product } i}{\text{total moles of products}} \times 100 \quad (2)$$

Additionally, the percentage of HDO and DCO/DCO_2 reactions were calculated according to Equations (3) and (4), respectively [29].

$$HDO = \frac{\text{total moles of n} - \text{alkanes } (nC_{16} + nC_{18} + nC_{20} + nC_{22}) \text{ in products}}{\text{total moles of fatty acid } (nC_{16} + nC_{18} + nC_{20} + nC_{22}) \text{in WCO}} \times 100 \quad (3)$$

$$DCO \Big/ DCO_2 = \frac{\text{total moles of n} - \text{alkanes } (nC_{15} + nC_{17} + nC_{19} + nC_{21}) \text{ in products}}{\text{total moles of fatty acid } (nC_{16} + nC_{18} + nC_{20} + nC_{22}) \text{in WCO}} \times 100 \quad (4)$$

3. Results

3.1. WCO characterization

The resulting WCO composition is showed in Table 1. As described, the oil is mainly composed by unsaturated C_{18} fatty acids (oleic and linoleic acid), and a minor part of saturated fatty acids (palmitic and stearic acid).

Table 1
Fatty acid composition of WCO.

Fatty Acid	Composition (wt. %)
Palmitic acid ($C_{16:0}$)	10.17
Stearic acid ($C_{18:0}$)	5.80
Oleic acid ($C_{18:1}$)	42.83
Linoleic acid ($C_{18:2}$)	38.96
Arachidic acid ($C_{20:0}$)	0.71
Gadoleic acid ($C_{20:1}$)	0.61
Behenic acid ($C_{22:0}$)	0.92

3.2. Catalysts characterization

XRD was performed aiming to assess the crystalline structure of the reduced catalysts. As depicted in Fig. 1a and b, respectively, Co-Mo/CNT and Co-Mo/CNT_{ox} presented a peak at 2θ = 26.0° [011], characteristic of the graphite structure of CNTs, and also a broad peak at 2θ = 43.5° due to the graphitized nature of the carbon material used. Moreover, peaks at 2θ = 37.1° and 53.5° assigned to the planes of [020] and [022]

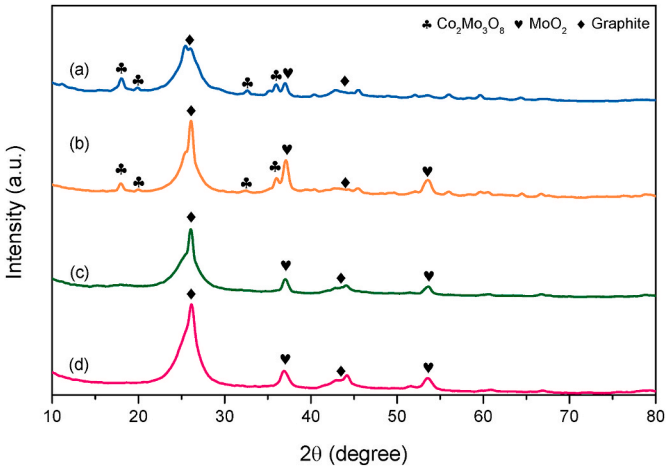

Fig. 1. XRD patterns of (a) Co-Mo/CNT, (b) Co-Mo/CNT_{ox}, (c) Ni-Mo/CNT and (d) Ni-Mo/CNT_{ox}.

of monoclinic MoO_2 were identified, respectively [26]. An interaction between Co and Mo was observed as an oxide species corresponding to $Co_2Mo_3O_8$ (2θ = 17.9° [002], 19.9° [101], 25.3° [102] and 35.7° [200]) [30,31]. Shang et al. [32] also synthesized Co and Mo catalysts supported on commercial CNTs for hydrotreatment applications. The authors observed that above 6 wt% Mo, peaks relating to monoclinic MoO_2 were apparent in the XRD patterns, indicating the presence of Mo oxide agglomerates. Regarding Ni-Mo catalysts, as shown in Fig. 1c and d, MoO_2 and the graphite structure of CNTs were the only crystalline phases identified in the XRD patterns. No evident peaks of Ni were detected, indicating that Ni species are finely dispersed. Moreover, no evident interactions of Ni and Mo were found by the XRD analysis as observed in Co-Mo catalysts. XRD pattern of Co-Mo/Al_2O_3 is shown in Fig. S1. The commercial catalyst presented a lower crystallinity compared to the CNT-based Co-Mo catalysts, with small reflections associated to $Co_2Mo_3O_8$ and Mo oxides.

TEM images of Co-Mo/CNT_{ox} and Ni-Mo/CNT_{ox} are depicted in Fig. 2. Fig. 2a–d revealed that metal particles are located on the surface of CNT_{ox}. Higher magnification images show the presence of particles inside the tubes (Fig. 2b, c, 2d and 2f). By -STEM with EDS analysis (Figs. S2, S3a and S3b), it is possible to confirm the presence of Mo in the inner cavities of the CNTs, proving that the tips of the CNTs were open during the oxidation treatment. According to Li et al. [33], at the

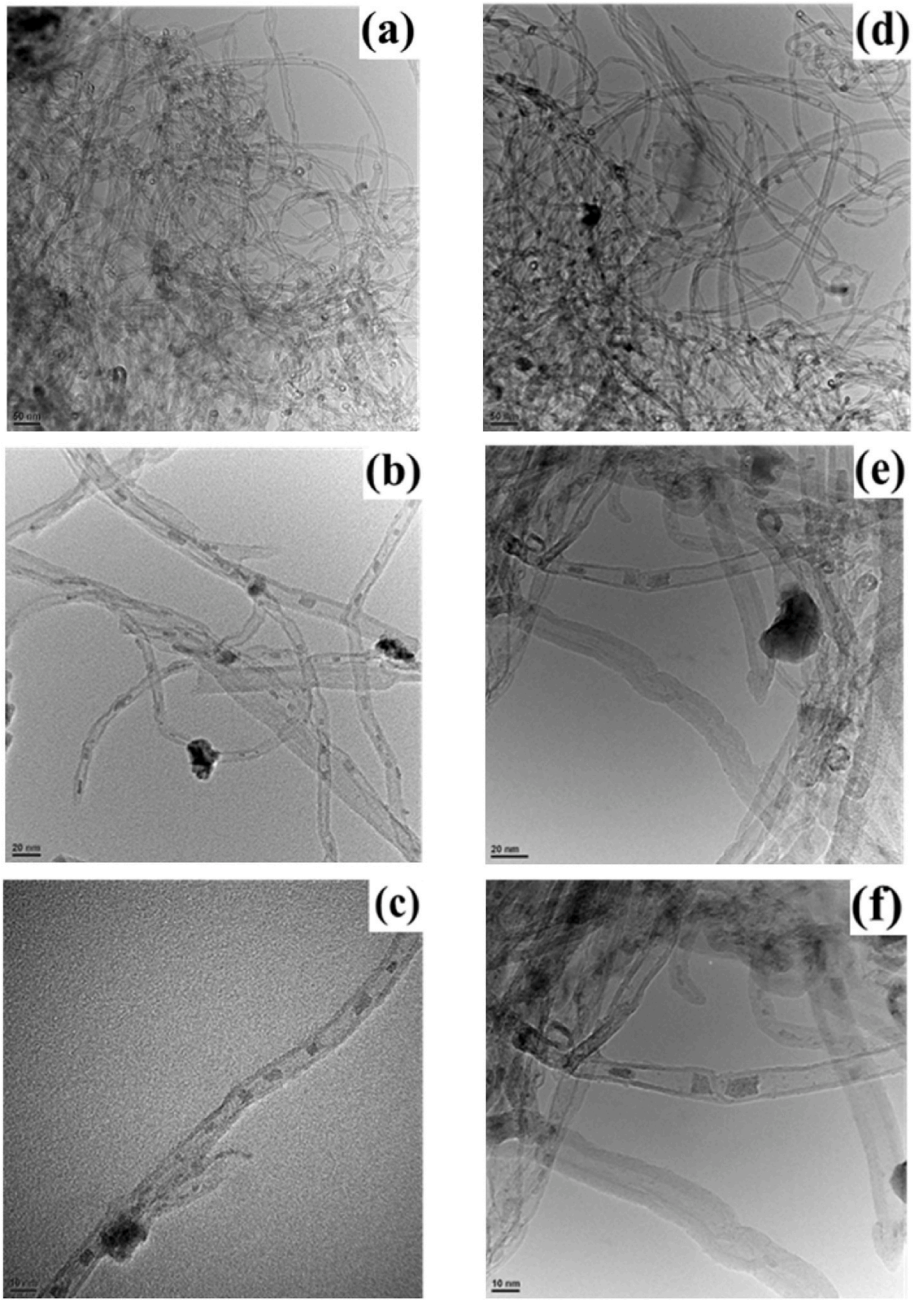

Fig. 2. TEM images of Co-Mo/CNT_{ox} (a, b and c) and Ni-Mo/CNT_{ox} (d, e and f).

temperature of 600 °C, MoO_3 interdiffuses with carbon atoms originating from the defect sites of CNTs after the oxidation step, leading to the formation of MoO_2. Additionally, Fig. S3c shows the presence of encapsulated Fe inside the tubes, indicating that the oxidative treatment used was insufficient to completely remove the metallic impurities associated with the production method of the commercial CNTs. It is also noted that Ni or Co particles are always associated with Mo on the surface of the CNT_{ox} in both catalysts (Figs. S3a and S3d). XRD analysis assigned that an alloy formed between Co and Mo ($Co_2Mo_3O_8$), while no Ni crystal structures were identified, suggesting that the Ni particles may have dispersed in the MoO_2 formed after the catalysts were reduced.

The chemical composition of each catalyst is outlined in Table 2. The values obtained for N and S were minimal, comprising less than 0.5 wt. %. Additionally, the inorganic matter, excluding the metals impregnated in the support, is referred to as "Other compounds." The metals' content obtained by ICP-OES is in accordance with the nominal metal loadings. Regarding the elemental analysis, results suggest that, once an increase in oxygen content from 1.8 to 4.4 wt. % was noted, the oxidative treatment of CNTs was successful in introducing oxygenated groups on the support surface. Nevertheless, after preparing the carbon supported catalysts, the treatment and the reducing temperatures were enough to decompose some oxygen-containing groups, explaining the similar O content. Overall, acid groups such as carboxylic acids decomposed at low temperatures (200–450 °C), followed by carboxylic anhydrides (400–600 °C) and lactones at high temperatures (550–700 °C) [34,35]. To investigate how this effect influenced the acidity of the catalysts, titration tests were carried out to determine the total acidity of the materials. As seen in Table 3, after the oxidation treatment with HNO_3, total acidity doubled from 1.7 to 3.4 mmol H^+ g_{cat}^{-1}, corroborating with the results obtained in the elemental analysis. Although the temperature used in the heat treatment of the catalysts contributed to the removal of oxygenated groups, it was observed that the acidity values for all the

Table 2
Chemical composition of the catalysts and supports.

Sample	C (wt. %)[a]	H (wt. %)[a]	O (wt. %)[a]	Co (wt. %)[b]	Ni (wt. %)[b]	Mo (wt. %)[b]	Other compounds (%)
CNT	89.8	0.4	1.8	–	–	–	8.0
CNT_{ox}	93.4	1.4	4.4	–	–	–	0.8
Co-Mo/CNT	69.5	0.6	8.9	1.4	–	10.0	9.6
Co-Mo/CNT_{ox}	76.4	0.6	9.2	1.4	–	10.3	2.1
Ni-Mo/CNT	74.3	0.3	7.2	–	2.2	10.7	5.3
Ni-Mo/CNT_{ox}	82.3	0.3	5.9	–	2.3	10.9	–
Co-Mo/Al_2O_3	0.3	1.3	16.2	2.5	–	10.5	69.2

[a] Elemental analysis.
[b] ICP-OES.

Table 3
Textural properties and acidity of the catalysts and supports.

Sample	$S_{BET} \pm 10$ ($m^2\ g^{-1}$)	$S_{ext} \pm 10$ ($m^2\ g^{-1}$)	$V_p \pm 0.02$ ($cm^3\ g^{-1}$)	Total acidity ± 0.2 (mmol $H^+\ g_{cat}^{-1}$)
CNT	229	229	1.54	1.7
CNT_{ox}	262	262	1.44	3.4
Co-Mo/CNT	198	198	1.51	3.2
Co-Mo/CNT_{ox}	227	227	1.24	2.9
Ni-Mo/CNT	201	201	1.55	3.1
Ni-Mo/CNT_{ox}	199	199	1.28	3.0
Co-Mo/Al_2O_3	247	247	0.42	2.5

catalysts synthesized were around 3 mmol $H^+\ g_{cat}^{-1}$. This indicates that the increase and/or the maintenance of acidity compared to the support used is attributed to the formation of acid sites on the surface of the material by the formation of the metal oxides identified in the XRD. In addition, the commercial catalyst is the catalyst with less acidity since alumina is a material with lower-moderate acidity [36].

Subsequently, the textural properties were assessed by N_2 adsorption-desorption at - 196 °C (Table 3). All the catalysts had no micropores, implying that these materials are primarily mesoporous. The catalysts and the supports isotherms are illustrated in Fig. S4. Co-Mo and Ni-Mo catalysts supported on CNT and CNT_{ox} showed type II isotherm, whereas the Co-Mo/Al_2O_3 presented a type IV isotherm [37]. CNT_{ox} presented a higher BET area than the original CNT caused by the opening of the edges and bringing defects in the sidewalls and a slight reduction in the pore volumes due to the introduction of oxygen-containing groups [34]. Despite its high BET area, the commercial catalyst has a substantially lower pore volume compared with the carbon catalysts. After impregnating the metals on the surface of the supports, the BET area decreased, as expected. Although the pore volume of Co-Mo/CNT_{ox} and Ni-Mo/CNT_{ox} declined, the effect was not the same for Co-Mo/CNT and Ni-Mo/CNT. This indicates that the metals were delivered into the pores as a result of opening of the tips and the defects in the CNT sidewalls after the oxidation treatment, corroborating with TEM analysis, whereas metals are more concentrated on the surface of the material in CNT-based catalysts.

3.3. Catalytic reactions

The synthesized catalysts were then tested for the direct conversion of WCO into liquid products. For the sake of clearness, the data are split down into the carbon ranges of *n*-alkanes (C_5-C_7, C_8-C_{16}, and C_{17}-C_{22}), iso-alkanes, alkenes, octadecanal ($C_{18}H_{36}O$), and octadecanol ($C_{18}H_{38}O$), as illustrated in Fig. 3. Initially, a blank experiment was run in the absence of any catalyst to assess the background. The results showed a very low carbon conversion (5 mol.%) and the formation of practically only *n*-alkanes and a small amount of $C_{18}H_{36}O$. Since WCO is mainly composed of oleic and linoleic acids, it is expected a higher amount of C_{18} compounds as products derived by HDO reaction and C_{17} from DCO/DCO_2 reactions [29]. An additional test was carried out with the supports (CNT and CNT_{ox}) as catalysts to evaluate their contribution to the reaction. When CNT was used, a carbon conversion of 25.3 mol.% was achieved, while for the CNT_{ox} this conversion was 8.9 mol.%, similar to the blank experiment. The high presence of impurities from the production of the CNTs, mainly Fe, may have contributed to active sites, consequently increasing the carbon conversion. Iron-based catalysts were reported in the literature to be selective to hydrogenolysis of C–O and C=O in triglycerides and fatty acids [38,39]. Even though Fe particles were still identified in the CNT_{ox}, treatment with HNO_3 helped to remove most of these metals, which explains the similar performance to the blank test, thus confirming the lack of activity of the carbon materials on their own.

Regarding the Co-Mo/CNT based materials, both catalysts converted almost the same amount of WCO (around 50 mol.%), but with some differences in the distribution of liquid products. Overall, these catalysts presented a slight selectivity for gasoline (3–9 mol.% of C_5-C_7) and jet fuel range (10–14 mol.% of C_8-C_{16}), with a small percentage of iso-C_{13}-C_{18} (4 mol.%). However, the quantity of these hydrocarbon was minimal compared with the C_{17}-C_{22} range. The most prominent divergence is that Co-Mo/CNT_{ox} provided a higher selectivity for C_{16}-C_{18} alkenes (7.2 mol.%) compared to Co-Mo/CNT (1.5 mol.%). Besides the comparable physical-chemical features displayed in both catalysts, TEM analysis indicated that Co-Mo/CNT_{ox} showed a higher presence of MoO_2 particles, mainly inside the tubes, decreasing the CNTs inner cavity. This fact could contribute to an intense interaction between the metal particles

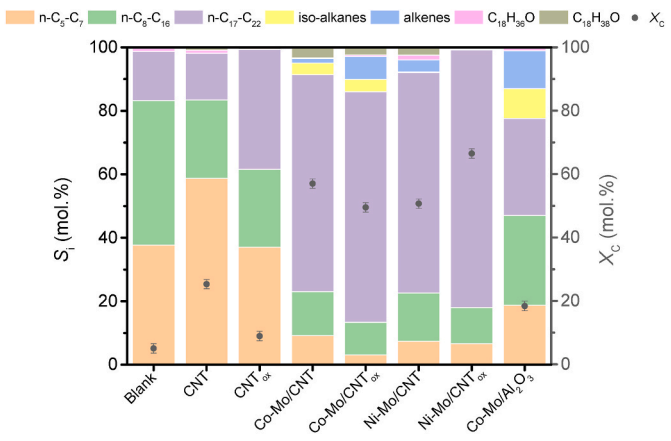

Fig. 3. Liquid products distribution of WCO deoxygenation reactions over different catalysts. Reaction Conditions: 350 °C, 70 bar H_2 (at room temperature), 1000 rpm, 3 h, 0.25 g of catalyst, 2.5 g of WCO, 25 g of n-decane.

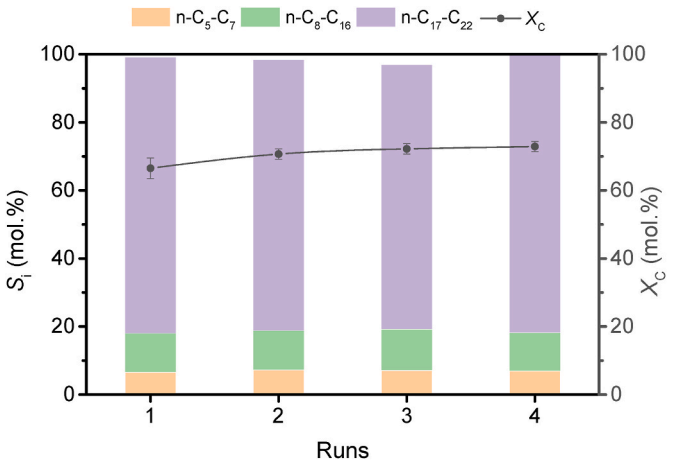

Fig. 4. Liquid products distribution after four consecutive runs with Ni-Mo/CNT_{ox}. Reaction Conditions: 350 °C, 70 bar H_2 (at room temperature), 1000 rpm, 3 h, 0.25 g of catalyst, 2.5 g of WCO, 25 g of n-decane.

and the alkenes molecules for this catalyst, while the total amount of *n*-alkanes in the products distribution is lower and no alkenes were produced using only the CNT_{ox}.

Whereas Ni-Mo/CNT presented a similar activity to the Co-Mo/CNT catalyst, Ni-Mo/CNT_{ox} showed the best catalytic performance among the materials tested. No oxygenated intermediates such as $C_{18}H_{36}O$ and $C_{18}H_{38}O$ were identified. A plausible explanation is that the presence of a Co-Mo alloy (detected by XRD) was not as beneficial as having separate Ni and Mo particles. Although the oxidation of CNTs facilitated the dispersion of the metals, this effect was only observed for the Ni catalysts. Consequently, the dispersion of Ni particles on the CNT_{ox} support was higher, as expected, leading to increased selectivity for *n*-alkanes at the end of the 3 h of reaction.

In the reaction conditions used in this work, the catalytic performance of the commercial Co-Mo/Al_2O_3 catalyst was inferior compared to the CNT-based catalysts, converting only 17.7 mol.% of the WCO. It is possible that the lower total pore volume and crystallinity of Co-Mo/Al_2O_3 compared with the CNT-based catalysts contributed to this lower conversion.

Since Ni-Mo/CNT_{ox} performed better in terms of selectivity to diesel range hydrocarbons, recyclability tests were carried out, as shown in Fig. 4, where four runs were performed under the same conditions. After each cycle, the catalyst was recovered by filtration, being properly washed several times with acetone and dried overnight in an oven at 110 °C for the next catalytic run. It was noted that Ni-Mo/CNT_{ox} was highly stable, as there was no noticeable decline in the conversion and selectivity values of the products. Overall, CNTs have superior stability in hydroprocessing reactions of lipid sources compared with other inorganic supports, mainly zeolites that tend to deactivate faster [40–42]. On the other hand, Ding et al. [26] performed a cycling experiment using MoO_2/CNT catalysts for five consecutive runs to evaluate palmitic acid deoxygenation reaction and no significant change in the catalyst activity was observed. In further studies, the same authors investigated the same reaction using a Co-doped MoO_2/CNT catalyst which showed a high stability until the fifth cycle [43]. Yang et al. [20] studied the HDO of Jatropha oil and concluded that, after five cycles, the carbon disposition over their Ni-phosphomolybdic acid supported on CNT were minimal, and no substantial decrease in the conversion and in the yields of C_{15}-C_{18} hydrocarbons was observed.

As described, the formation of alkenes and other intermediate oxygenated compounds was still observed on the Co-Mo catalysts supported on CNTs. To verify whether these compounds could eventually be converted into *n*-alkanes or other products, we decided to increase the reaction time to 5 h. The results of the liquid and gaseous products of the Co-Mo/CNT and Co-Mo/CNT_{ox} catalysts are shown in Fig. 5. In general, the distribution of liquid and gaseous products is similar for both catalysts used and the increase in reaction time contributed to the conversion of reaction intermediates into *n*-alkanes, mainly in the C_{17} to C_{22} range for Co-Mo/CNT_{ox} (Fig. 5b). The iso-C_{17}-C_{22} were produced at the beginning of the reaction and remained unchanged for both catalysts after 5 h, indicating that no further cracking into smaller hydrocarbons occurred. Regarding the gas phase, it was observed an increase in the CH_4 amount, indicating a rise in the cracking of small compounds (e.g., propane, ethane and C_6 products). Data for propylene and C_{6+} are reported in the graphics as "Others". Typically, the values C_{6+} remained

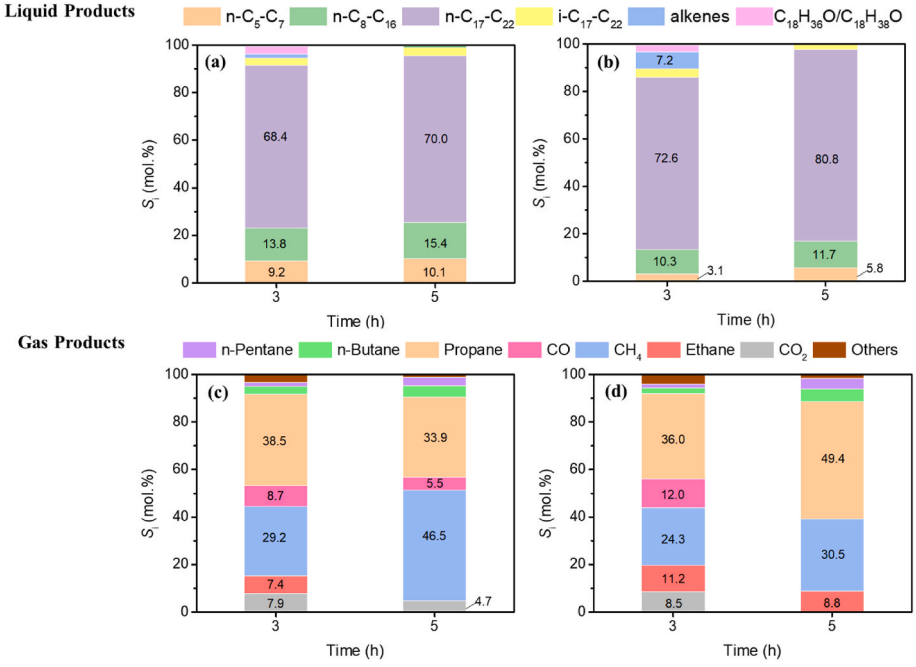

Fig. 5. Liquid products and gas products distribution of WCO deoxygenation reactions over Co-Mo/CNT (a and c) and Co-Mo/CNT_{ox} (b and d). Reaction conditions: 350 °C, 70 bar H_2 (at room temperature), 1000 rpm, 3–5 h, 0.25 g of catalyst, 2.5 g of WCO, 25 g of *n*-decane.

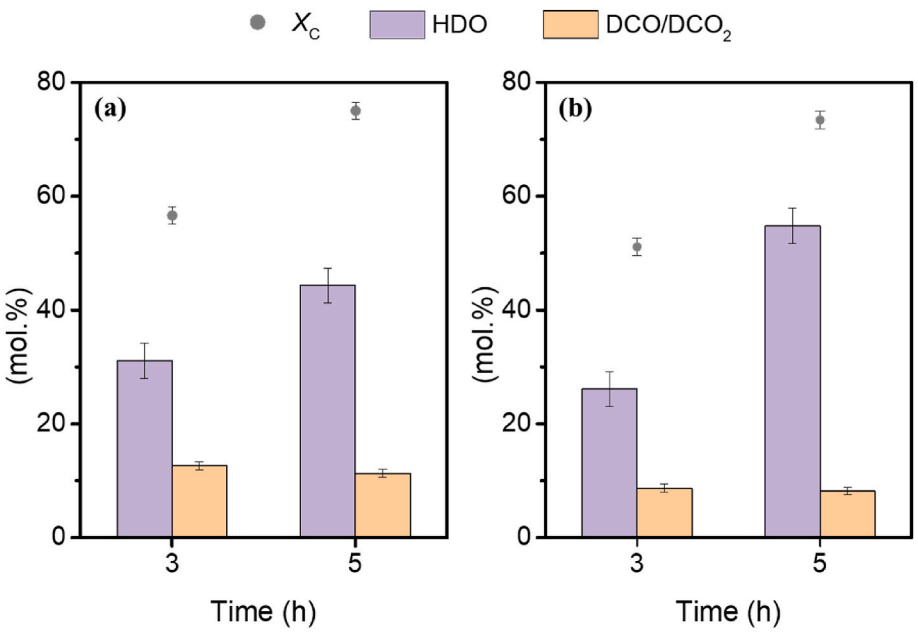

Fig. 6. Evolution of the conversion, HDO and DCO/DCO$_2$ through the time over (a) Co-Mo/CNT and (b) Co-Mo/CNT$_{ox}$. Reaction conditions: 350 °C, 70 bar H_2 (at room temperature), 1000 rpm, 3–5 h, 0.25 g of catalyst, 2.5 g of WCO, 25 g of n-decane.

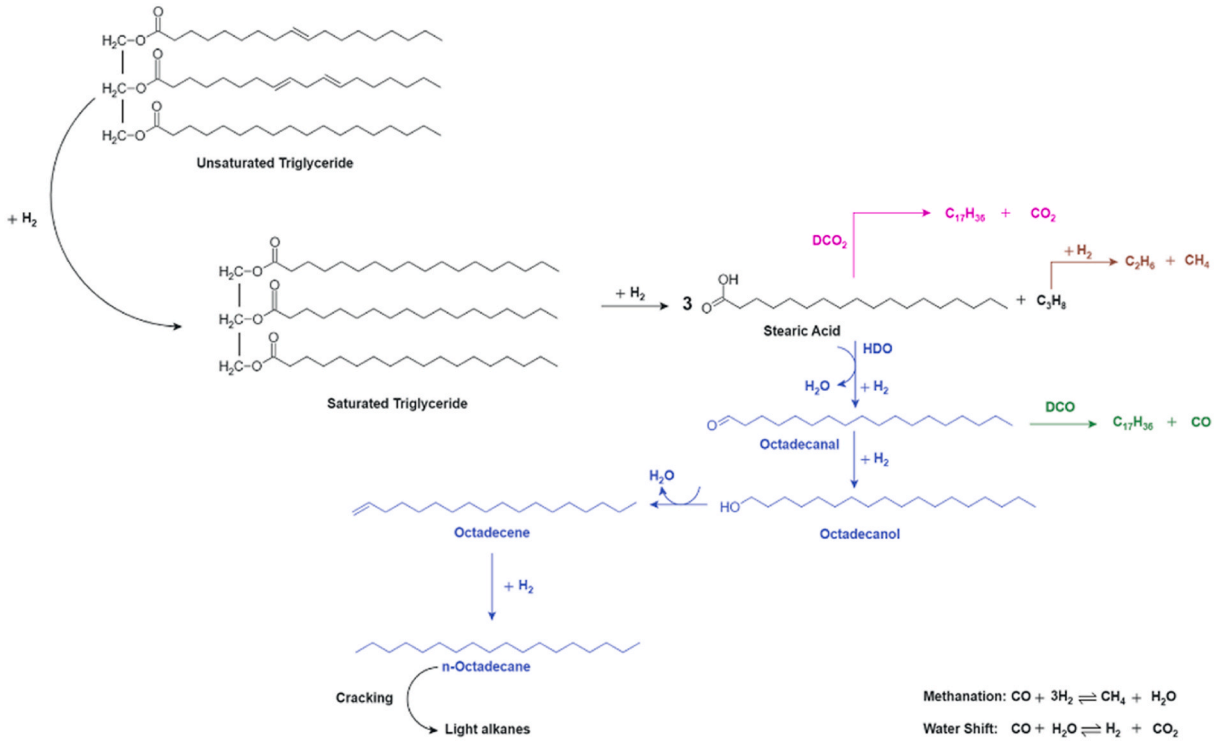

Fig. 7. Proposed pathway to convert WCO into liquid fuels over Co-Mo/CNT catalysts.

unchanged at around 2.0 mol.% while propylene almost disappears for both Co-Mo catalysts. According to Fig. 6, the increase in carbon conversion to about 75 mol.% after 5 h was mainly via HDO, with an increase of approximately 28 mol.% for Co-Mo/CNT (Figs. 6a) and 13 mol.% for Co-Mo/CNT$_{ox}$ (Fig. 6b). However, the DCO/DCO$_2$ values remained unchanged as the reaction time increased (around 12 mol.% and 8 mol.% for Co-Mo/CNT and Co-Mo/CNT$_{ox}$, respectively).

Considering these results, a possible reaction pathway was proposed for the conversion of WCO (Fig. 7). As HDO is more interesting from an environmental point of view, the proposed route was based on the catalyst that promoted the highest percentage of this route (i.e., Co-Mo/CNT$_{ox}$). Firstly, unsaturated triglycerides containing in the WCO, such as oleic, linoleic and gadoleic acids, are hydrogenated into saturated triglycerides [44]. In sequence, all the saturated triglycerides are hydrogenated, producing the corresponding free fatty acid (FFA) and a molecule of propane. The saturated fatty acid is deoxygenated by two possible routes: HDO or DCO/DCO$_2$. In HDO, the corresponding aldehyde is formed followed by its hydrogenation, producing an alcohol

(confirmed by the presence of $C_{18}H_{36}O$ and $C_{18}H_{38}O$), which is subsequently hydrodeoxygenated to the corresponding *n*-alkane (C_{16}, C_{18}, C_{20} and C_{22}) [20,26]. In this case, FFA is completed deoxygenated to the corresponding *n*-alkane removing a molecule of water. On the other hand, in DCO/DCO_2, to obtain *n*-alkanes (C_{15}, C_{17}, C_{19} and C_{21}), FFA deoxygenation occurs by eliminating CO or CO_2. Hydrocracking can also happen producing $< C_{14}$ alkanes, in the presence of high temperature and pressure [44,45]. Moreover, the propane produced is cracked into ethane (C_2H_6) and methane (CH_4). The formed CO and CO_2 by DCO/DCO_2 routes are involved in reversible reactions with the H_2 to form more CH_4 and water (methanation and water shift reactions) [46]. The reaction pathway described aligns with previous studies reported in the literature on CNT-based catalysts. However, the pathway remains unchanged whether using the CNT or CNT_{ox} catalyst. On the other hand, due to the higher concentration of MoO_2 species in bimetallic catalysts, the HDO pathway dominates, as also noted by Ding et al. [26]. In contrast, for monometallic catalysts such as Ni/CNT and Ni-phosphomolybdic acid/CNT, the DCO/DCO_2 pathway was found to be predominant [20,47].

4. Conclusions

In this study, Co-Mo and Ni-Mo catalysts supported on CNT and CNT_{ox} were synthesized to evaluate their effectiveness in converting WCO into liquid fuels. The results demonstrated the production of various hydrocarbons, in the range of transport fuels, from gasoline, jet fuel and diesel constituents. The catalysts supported on CNT_{ox} did not show significant differences compared to those supported on CNT, as the thermal treatment temperatures were excessively high, eliminating the acidic oxygenated groups from the CNTs surface. Among the tested catalysts, Ni-Mo/CNT_{ox} emerged as the most efficient for converting WCO, particularly into diesel products. However, the bimetallic Co-Mo/CNT catalysts required a longer reaction time (totaling 5 h) to enhance the conversion and formation of *n*-alkanes. The predominant deoxygenation route observed was HDO, which is the most desirable pathway for deoxygenating renewable lipid sources, as it avoids the production of CO and CO_2.

CRediT authorship contribution statement

K.K. Ferreira: Writing – review & editing, Writing – original draft, Visualization, Validation, Methodology, Investigation, Formal analysis, Data curation. **C. Di Stasi:** Writing – review & editing, Visualization, Validation, Methodology, Investigation, Formal analysis, Data curation, Conceptualization. **A. Ayala-Cortés:** Writing – review & editing, Visualization, Validation, Methodology, Investigation, Formal analysis, Data curation, Conceptualization. **L.S. Ribeiro:** Writing – review & editing, Supervision, Methodology, Conceptualization. **J.L. Pinilla:** Writing – review & editing, Supervision, Resources, Methodology, Funding acquisition, Conceptualization. **I. Suelves:** Writing – review & editing, Supervision, Resources, Methodology, Funding acquisition, Conceptualization. **M.F.R. Pereira:** Writing – review & editing, Supervision, Resources, Methodology, Funding acquisition.

Data availability statement

The original contributions presented in the study are included in the article/supplementary material.

Declaration of competing interest

The authors declare that they have no known competing financial interests or personal relationships that could have appeared to influence the work reported in this paper.

Acknowledgments

This work was supported by national funds through FCT/MCTES (PIDDAC): LSRE-LCM, UIDB/50020/2020 (DOI: 10.54499/UIDB/50020/2020) and UIDP/50020/2020 (DOI: 10.54499/UIDP/50020/2020); and ALiCE, LA/P/0045/2020 (DOI: 10.54499/LA/P/0045/2020). The authors are grateful for the financial support from the I + D + i project PID2020-115053RB-I00, funded by Spanish Ministry of Science and Innovation (MCIN/AEI/10.13039/501100011033). The authors also thank Gobierno de Aragón (DGA) for the financial support to Grupo de Conversión de Combustibles (T06_23). K. K. Ferreira acknowledges her Ph.D. scholarship (2022.12949.BD) from FCT. C.D.S is grateful for the Juan de la Cierva (JdC) fellowship (Grant Number: JDC2022-048765-I) funded by MICIU/AEI/10.13039/501100011033 and by FSE+. The authors acknowledge the use of instrumentation as well as the technical advice provided by the National Facility ELECMI ICTS, node Laboratorio de Microscopias Avanzadas (LMA) at Universidad de Zaragoza and the Analysis and Characterization service at ICB-CSIC. The authors also thank Naturalmente Social Recikla, S. L., for providing the waste cooking oil used in this work.

Appendix A. Supplementary data

Supplementary data to this article can be found online at https://doi.org/10.1016/j.biombioe.2024.107480.

Data availability

Data will be made available on request.

References

[1] J. Teter, F. Voswinkel, International energy agency, Transport (2023). https://www.iea.org/energysystem/transport. (Accessed 26 April 2024), 2023.
[2] J. Sun, Y. Li, C. Mu, J. Wei, Y. Zhao, X. Ma, S. Wang, Supported heteropolyacids catalysts for the selective hydrocracking and isomerization of n-C16 to produce jet fuel, Appl. Catal. Gen. 598 (2020), https://doi.org/10.1016/j.apcata.2020.117556.
[3] Z. Ullah, M.A. Bustam, Z. Man, Biodiesel production from waste cooking oil by acidic ionic liquid as a catalyst, Renew. Energy 77 (2015) 521–526, https://doi.org/10.1016/j.renene.2014.12.040.
[4] M.G. Kulkarni, A.K. Dalai, Waste cooking oil - an economical source for biodiesel: a review, Ind. Eng. Chem. Res. 45 (2006) 2901–2913, https://doi.org/10.1021/ie0510526.
[5] L. Rocha-Meneses, A. Hari, A. Inayat, L.A. Yousef, S. Alarab, M. Abdallah, A. Shanableh, C. Ghenai, S. Shanmugam, T. Kikas, Recent advances on biodiesel production from waste cooking oil (WCO): a review of reactors, catalysts, and optimization techniques impacting the production, Fuel 348 (2023), https://doi.org/10.1016/j.fuel.2023.128514.
[6] M.U.H. Suzihaque, N. Syazwina, H. Alwi, U.K. Ibrahim, S. Abdullah, N. Haron, A sustainability study of the processing of kitchen waste as a potential source of biofuel: biodiesel production from waste cooking oil (WCO), Mater. Today Proc. 63 (2022) S484–S489, https://doi.org/10.1016/j.matpr.2022.04.526.
[7] T. Li, J. Cheng, R. Huang, J. Zhou, K. Cen, Conversion of waste cooking oil to jet biofuel with nickel-based mesoporous zeolite Y catalyst, Bioresour. Technol. 197 (2015) 289–294, https://doi.org/10.1016/j.biortech.2015.08.115.
[8] N. Le-Phuc, T.V. Tran, T.T. Phan, P.T. Ngo, Q.L.M. Ha, T.N. Luong, T.H. Tran, T. T. Phan, High-efficient production of biofuels using spent fluid catalytic cracking (FCC) catalysts and high acid value waste cooking oils, Renew. Energy 168 (2021) 57–63, https://doi.org/10.1016/j.renene.2020.12.050.
[9] R. Saravanan, T. Sathish, Ü. Ağbulut, R. Sathyamurthy, P. Sharma, E. Linul, M. Asif, Waste bull bone based reusable and biodegradable heterogeneous catalyst for alternate fuel production from WCO, and investigation of its usability as fuel substitute, Fuel 355 (2024), https://doi.org/10.1016/j.fuel.2023.129436.
[10] D. Verma, R. Kumar, B.S. Rana, A.K. Sinha, Aviation fuel production from lipids by a single-step route using hierarchical mesoporous zeolites, Energy Environ. Sci. 4 (2011) 1667–1671, https://doi.org/10.1039/c0ee00744g.
[11] M. Rabaev, M.V. Landau, R. Vidruk-Nehemya, V. Koukouliev, R. Zarchin, M. Herskowitz, Conversion of vegetable oils on Pt/Al2O3/SAPO-11 to diesel and jet fuels containing aromatics, Fuel 161 (2015) 287–294, https://doi.org/10.1016/j.fuel.2015.08.063.
[12] P.M. Yeletsky, R.G. Kukushkin, V.A. Yakovlev, B.H. Chen, Recent advances in one-stage conversion of lipid-based biomass-derived oils into fuel components – aromatics and isomerized alkanes, Fuel 278 (2020), https://doi.org/10.1016/j.fuel.2020.118255.

[13] P. Mäki-Arvela, M. Martínez-Klimov, D.Y. Murzin, Hydroconversion of fatty acids and vegetable oils for production of jet fuels, Fuel 306 (2021), https://doi.org/10.1016/j.fuel.2021.121673.
[14] M.X.Y. Ravindran, N. Asikin-Mijan, G. AbdulKareem-Alsultan, H.C. Ong, M. M. Nurfarhana, H.V. Lee, T.A. Kurniawan, D. Derawi, S.F.M. Yusoff, I.M. Lokman, Y.H. Taufiq-Yap, A review of carbon-based catalyst for production of renewable hydrocarbon rich fuel, J. Environ. Chem. Eng. 12 (2024), https://doi.org/10.1016/j.jece.2024.112330.
[15] S. Karatzos, J.S. van Dyk, J.D. McMillan, J. Saddler, Drop-in biofuel production via conventional (lipid/fatty acid) and advanced (biomass) routes. Part I, Biofuels, Bioprod. and Bioref. 11 (2017) 344–362, https://doi.org/10.1002/bbb.1746.
[16] S. Lycourghiotis, E. Kordouli, K. Bourikas, C. Kordulis, A. Lycourghiotis, The role of promoters in metallic nickel catalysts used for green diesel production: a critical review, Fuel Process. Technol. 244 (2023), https://doi.org/10.1016/j.fuproc.2023.107690.
[17] M. Attia, S. Farag, J. Chaouki, Upgrading of oils from biomass and waste: catalytic hydrodeoxygenation, Catalysts 10 (2020) 1–30, https://doi.org/10.3390/catal10121381.
[18] V. Georgakilas, J.A. Perman, J. Tucek, R. Zboril, Broad family of carbon nanoallotropes: classification, chemistry, and applications of fullerenes, carbon dots, nanotubes, graphene, nanodiamonds, and combined superstructures, Chem. Rev. 115 (2015) 4744–4822, https://doi.org/10.1021/cr500304f.
[19] J.L. Pinilla, H. Purón, D. Torres, S. De Llobet, R. Moliner, I. Suelves, M. Millan, Carbon nanofibres coated with Ni decorated MoS2 nanosheets as catalyst for vacuum residue hydroprocessing, Appl. Catal., B 148–149 (2014) 357–365, https://doi.org/10.1016/j.apcatb.2013.11.019.
[20] X. Yang, X. Li, J. Liu, L. Rong, Ni/phosphomolybdic acid immobilized on carbon nanotubes for catalytic cracking of Jatropha oil, Chem. Phys. Lett. 720 (2019) 42–51, https://doi.org/10.1016/j.cplett.2019.02.008.
[21] E. Pérez-Mayoral, V. Calvino-Casilda, E. Soriano, Metal-supported carbon-based materials: opportunities and challenges in the synthesis of valuable products, Catal. Sci. Technol. 6 (2016) 1265–1291, https://doi.org/10.1039/c5cy01437a.
[22] D. Verma, R. Kumar, B.S. Rana, A.K. Sinha, Aviation fuel production from lipids by a single-step route using hierarchical mesoporous zeolites, Energy Environ. Sci. 4 (2011) 1667–1671, https://doi.org/10.1039/c0ee00744g.
[23] U. Shafihi, R.S.R.M. Hafriz, N.A. Arifin, I. Nor Shafizah, A. Idris, A. Salmiaton, N. M. Razali, Catalytic deoxygenation with SO42–Fe2O3/Al2O3 catalyst: optimization by Taguchi method, Results Eng. 17 (2023), https://doi.org/10.1016/j.rineng.2023.100959.
[24] G.A. Alsultan, N. Asikin-Mijan, H.V. Lee, A.S. Albazzaz, Y.H. Taufiq-Yap, Deoxygenation of waste cooking to renewable diesel over walnut shell-derived nanorode activated carbon supported CaO-La2O3 catalyst, Energy Convers. Manag. 151 (2017) 311–323, https://doi.org/10.1016/j.enconman.2017.09.001.
[25] P.J. Ahranjani, S.F. Saei, G.A. El-Hiti, K.K. Yadav, J. Cho, S. Rezania, Magnetic carbon nanotubes doped cadmium oxide as heterogeneous catalyst for biodiesel from waste cooking oil, Chem. Eng. Res. Des. 201 (2024) 176–184, https://doi.org/10.1016/j.cherd.2023.11.059.
[26] R. Ding, Y. Wu, Y. Chen, J. Liang, J. Liu, M. Yang, Effective hydrodeoxygenation of palmitic acid to diesel-like hydrocarbons over MoO2/CNTs catalyst, Chem. Eng. Sci. 135 (2015) 517–525, https://doi.org/10.1016/j.ces.2014.10.024.
[27] A.B. Dongil, I.T. Ghampson, R. García, J.L.G. Fierro, N. Escalona, Hydrodeoxygenation of guaiacol over Ni/carbon catalysts: effect of the support and Ni loading, RSC Adv. 6 (2016) 2611–2623, https://doi.org/10.1039/c5ra22540j.
[28] P. De Filippis, C. Giavarini A, M. Scarsella, M. Sorrentino, Transesterification Processes for Vegetable Oils: a Simple Control Method of Methyl Ester Content, J. Am. Oil Chem. Soc. 72 (1995) 1399–1404, https://doi.org/10.1007/BF02546218.
[29] A.K. Noriega, A. Tirado, C. Méndez, G. Marroquín, J. Ancheyta, Hydrodeoxygenation of vegetable oil in batch reactor: experimental considerations, Chin. J. Chem. Eng. 28 (2020) 1670–1683, https://doi.org/10.1016/j.cjche.2019.12.022.
[30] O. Hassel, H. Mark, Über die Kristallstruktur des Graphits, Z. Phys. 25 (1924) 317–337, https://doi.org/10.1007/BF01327534.
[31] C. Xu, P. Chang, Z. Liu, L. Guan, X. Wang, J. Tao, Electrochemical activated molybdenum oxides based multiphase heterostructures with high hydrogen evolution activity in alkaline condition, J. Nanotechnol. 34 (2023), https://doi.org/10.1088/1361-6528/acefd9.
[32] H. Shang, C. Liu, Y. Xu, J. Qiu, F. Wei, States of carbon nanotube supported Mo-based HDS catalysts, Fuel Process. Technol. 88 (2007) 117–123, https://doi.org/10.1016/j.fuproc.2004.08.010.
[33] Z. Li, X. Wang, D. Li, H. Zhang, B. Zhang, Simultaneously enhanced electro-mechanical properties of CNTs/Cu-20wt.%Mo composite material by regulating interface with Mo2C nanoparticles, Diam. Relat. Mater. 147 (2024), https://doi.org/10.1016/j.diamond.2024.111315.
[34] L.S. Ribeiro, J.J. Delgado, J.J. de Melo Órfão, M.F. Ribeiro Pereira, Influence of the surface chemistry of multiwalled carbon nanotubes on the selective conversion of cellulose into sorbitol, ChemCatChem 9 (2017) 888–896, https://doi.org/10.1002/cctc.201601224.
[35] J.L. Figueiredo, M.F.R. Pereira, M.M.A. Freitas, J.J.M. Órfão, Modification of the surface chemistry of activated carbons, Carbon 37 (1999) 1379–1389, https://doi.org/10.1016/S0008-3816223(98)00333-9.
[36] S. Khan, A.N. Kay Lup, K.M. Qureshi, F. Abnisa, W.M.A. Wan Daud, M.F.A. Patah, A review on deoxygenation of triglycerides for jet fuel range hydrocarbons, J. Anal. Appl. Pyrolysis 140 (2019) 1–24, https://doi.org/10.1016/j.jaap.2019.03.005.
[37] J.L. Figueiredo, F.R. Ribeiro, Catálise Heterogênea, 2ª, Fundação Calouste Gulbenkian, 2007. Lisboa.
[38] S. Khan, K.M. Qureshi, A.N. Kay Lup, M.F.A. Patah, W.M.A. Wan Daud, Role of Ni–Fe/ZSM-5/SAPO-11 bifunctional catalyst on hydrodeoxygenation of palm oil and triolein for alternative jet fuel production, Biomass Bioenergy 164 (2022), https://doi.org/10.1016/j.biombioe.2022.106563.
[39] A.A. Ayandiran, P.E. Boahene, S. Nanda, A.K. Dalai, Y. Hu, Hydroprocessing of oleic acid for the production of aviation turbine fuel range hydrocarbons over bimetallic Fe-Cu/SiO2-Al2O3 catalysts promoted by Sn, Ti and Zr, J. Mol. Catal. 523 (2022), https://doi.org/10.1016/j.mcat.2020.111358.
[40] X. Li, M. Lin, R. Li, Q. Lu, M. Yang, Y. Wu, Preparation of Metal-Acid bifunctional catalyst Ni/ZSM-22 for palmitic acid catalytic deoxygenation, Fuel 332 (2023), https://doi.org/10.1016/j.fuel.2022.126139.
[41] T. Cordero-Lanzac, R. Palos, I. Hita, J.M. Arandes, J. Rodríguez-Mirasol, T. Cordero, J. Bilbao, P. Castaño, Revealing the pathways of catalyst deactivation by coke during the hydrodeoxygenation of raw bio-oil, Appl. Catal., B 239 (2018) 513–524, https://doi.org/10.1016/j.apcatb.2018.07.073.
[42] Z. Chen, X. Zhang, F. Yang, H. Peng, X. Zhang, S. Zhu, L. Che, Deactivation of a Y-zeolite based catalyst with coke evolution during the catalytic pyrolysis of polyethylene for fuel oil, Appl. Catal. Gen. 609 (2021), https://doi.org/10.1016/j.apcata.2020.117873.
[43] R. Ding, Y. Wu, Y. Chen, H. Chen, J. Wang, Y. Shi, M. Yang, Catalytic hydrodeoxygenation of palmitic acid over a bifunctional Co-doped MoO2/CNTs catalyst: an insight into the promoting effect of cobalt, Catal. Sci. Technol. 6 (2016) 2065–2076, https://doi.org/10.1039/c5cy01575h.
[44] V. Verma, A. Mishra, M. Anand, S.A. Farooqui, A.K. Sinha, Catalytic hydroprocessing of waste cooking oil for the production of drop-in aviation fuel and optimization for improving jet biofuel quality in a fixed bed reactor, Fuel 333 (2023), https://doi.org/10.1016/j.fuel.2022.126348.
[45] G.W. Huber, P. O'Connor, A. Corma, Processing biomass in conventional oil refineries: production of high quality diesel by hydrotreating vegetable oils in heavy vacuum oil mixtures, Appl. Catal. Gen. 329 (2007) 120–129, https://doi.org/10.1016/j.apcata.2007.07.002.
[46] S.K. Kim, S. Brand, H.S. Lee, Y. Kim, J. Kim, Production of renewable diesel by hydrotreatment of soybean oil: effect of reaction parameters, Chem. Eng. J. 228 (2013) 114–123, https://doi.org/10.1016/j.cej.2013.04.095.
[47] P. Duan, B. Wang, Y. Xu, Catalytic hydrothermal upgrading of crude bio-oils produced from different thermo-chemical conversion routes of microalgae, Bioresour. Technol. 186 (2015) 58–66, https://doi.org/10.1016/j.biortech.2015.03.050.